Korean J. Chem. Eng., 36(7), 1057-1068 (2019)
DOI: 10.1007/s11814-019-0284-0

pISSN: 0256-1115
eISSN: 1975-7220

Graphene/ternary layered double hydroxide composites: Efficient removal of anionic dye from aqueous phase

Taye Saheed Kazeem*, Mukarram Zubair, Muhammad Daud***, Nuhu Dalhat Mu'azu**, and Mamdouh Ahmed Al-Harthi*,****,†**

*Department of Chemical Engineering, King Fahd University of Petroleum & Minerals, Dhahran 31261, Saudi Arabia
**Department of Environmental Engineering, Imam Abdulrahman Bin Faisal University, Dammam 31982, Saudi Arabia
***Department of Chemical Engineering, University of Engineering and Technology, 25120 Peshawar, Pakistan
****Center of Research Excellence in Nanotechnology, King Fahd University of Petroleum & Minerals, 31261 Dhahran, Saudi Arabia

(*Received 6 November 2018 • accepted 27 April 2019*)

Abstract−Ternary layered double hydroxide, MgCoAl (MCA) and its graphene-based composite (G/MCA) were fabricated via a simple co-precipitation technique. The composites along with their calcined products (MCA-C) and (G/MCA-C) were used as adsorbents for the removal of an anionic dye, methyl orange (MO), from aqueous phase. The characterization results (scanning electron microscopy and transmission electron microscopy) revealed homogeneous dispersion of graphene onto the MCA. Calcination of G/MCA resulted in a rough and heterogeneous surface with significant improvement in oxygen functionalities and surface area, which plays a crucial role in improved dye adsorption performance. Adsorptive equilibrium was established at 240 min for MCA and G/MCA and 180 min for MCA-C and G/MCA-C respectively at pH 3 and optimum dosage of 10 mg. The Redlich-Peterson and Langmuir isotherm models closely describe the adsorption process with maximum adsorption capacities of 357.14, 384.62, 400.12 and 434.78 mg/g for MCA, G/MCA, MCA-C, and G/MCA-C respectively. Kinetics modeling indicates the adequacy and fitness of the pseudo-second-order model. A thermodynamics evaluation substantiates the exothermic nature of the adsorption processes. The MO-graphene ternary LDH composite adsorption process is controlled by several mechanisms including hydrogen bonding, surface adsorption, chemical and electrostatic interactions with surface reconstruction. The high removal efficiency of the MO coupled with high recovery and reusability of these nanomaterials showcases their potential for deployment in wastewater treatment.

Keywords: Methyl Orange, Graphene-ternary Layered Double Hydroxide, Adsorption Kinetics and Isotherm, Thermodynamics

INTRODUCTION

Contamination of water due to the presence of toxic pollutants is a serious worldwide problem. These pollutants are comprised of hazardous heavy metals, dyes, and organic compounds and are highly detrimental to both human health and ecosystems. Major pollutants in textile industry wastewater discharge are comprised of various synthetic dyes [1]. During the dyeing process, nearly 10-20% of unused dyes are directly discharged with the wastewater effluent. Hence, it becomes highly necessary to treat dye-containing wastewater to minimize the risk of environment pollution. Methyl orange (MO) is an anionic type of synthetic dye widely used in textiles production, printing and research laboratories [2]. Generally, synthetic dyes have a great tendency of lowering the oxygen level and light penetration in waters, and these pollution effects hinder both photosynthetic and biota growth. Direct contact of MO has been known for its mutagenic and carcinogenic effects among various health and environmental concerns [3].

There are various physio-chemical treatment schemes, such as flocculation and coagulation [4], ion exchange [5], chemical oxidation [6], and membrane filtration [7]. Among these, adsorption has become increasingly attractive for its simple operation, efficiency and affordability. Various synthesized adsorbents have been deployed for the elimination of dye contaminated-wastewater, among which are zeolite [8], bentonite [5], and activated carbon [9].

Despite the myriad of technologies associated with adsorbents, development of new adsorbents with profound adsorption capacities, large ion exchange, ease of regeneration and reuse is still an important quest. Layered double hydroxides (LDHs), which possess brucite-like layers, better known as hydrotalcite clays, have been garnering continuing recognition for their efficient use in water and wastewater treatment. This has been attributed to their large ion exchange capacities and specific surface areas [3]. LDHs are 2-D anionic clays which have a characteristic structural formula of $[M^{2+}_{1-x}M^{3+}_{x}(OH)_2]^{x+}(A^{n-})_{x/m}\cdot mH_2O$. M^{3+} stands for trivalent metals, while the M^{2+} represents the divalent cations, the A^{n-} is the intercalating anions and x is the molar ratio of trivalent cations ($0.2< x<0.33$) [3]. LDHs and their hybrids have been intensively used for removal of pollutants in water treatment [10]. Recently, ternary LDHs were being exploited due to their high sorption capacities

†To whom correspondence should be addressed.
E-mail: mamdouh@kfupm.edu.sa

[11]. Bharali and Deka [12] applied CuMgAl ternary LDH for the sorption of various dyes and reported excellent adsorption performance. They reported an increase in removal efficiency of methyl orange (MO) dye with increased Cu^{2+} composition ratio despite the reduction in surface area. They proposed that Cu^{2+} ratio induces lower basicity which contributes to the attraction between the dye molecules and LDH surface. Likewise, Zaghouane-Boudiaf and his team [11] removed methyl orange from the aqueous phase using uncalcined and calcined MgNiAl LDHs with higher adsorption found on the calcined sample. Lei et al. [13] reported the multifunctional performance of hierarchical NiMgAl ternary LDH for chromium and congo red (CR) removal. The maximum adsorption capacities for Cr(VI) and CR obtained were 103.4 mg/g and 1,250 mg/g, respectively.

Graphene, a 21st century-discovered 2D crystalline allotrope of carbon, with chicken-wire hexagonal structure [14] has gained continuing interest in different fields due to its strength (200 times stronger than steel), high surface area (~2,700 m^2/g) and tunable properties [15]. Therefore, graphene has been applied in supercapacitors, nanofillers, sensor, flame retardation and water treatment [15] to mention a few. The unique nanosized configuration of graphene endows its strong interaction with organic molecule coupled with fast equilibrium rate [16]. The nature of agglomeration in LDHs induces weak access to active sites, which may reduce performance. Hence, there is a need to hybridize with components which will serve as spacers to prevent such defects. Graphene with its unique compatibility with LDHs enhances accessibility to the active sites [17]. In addition, graphene/LDH composites have been reported to possess superior properties when compared to either LDHs or graphene [18]. In recent times, various graphene/LDH composites have been investigated for the effective elimination of dyes and heavy metals from water phase [10,15]. However, based on detailed literature review, to-date no work has been reported on the synthesis of graphene/ternary LDH as an adsorbent for the removal of anionic dyes. Previous studies demonstrated that using graphene as a substrate for LDHs [19,20] resulted in the prevention of aggregation in LDHs, enhancement in surface area and formation of mixed metal oxides on graphene sheets after subsequent calcination. Therefore, it is expected that coupling of graphene into layers of ternary LDH composites will improve the surface and structure characteristics and accelerates pollutants uptake from the water phase.

In this study, MgCoAl ternary LDH and graphene/MgCoAl composite were synthesized via a co-precipitation technique and investigated for aqueous adsorption of methyl orange (MO). FTIR, XRD, SEM, BET, and TGA were employed for the characterization of the composites. Investigation of various adsorption parameters on the removal of MO from the aqueous phase was carried out in batch adsorption study. Kinetic and equilibrium isotherm data were also fitted to various models to investigate the adsorptive rate-limiting step and mechanism. The possibility of regeneration and reuse of the adsorbents was also investigated for evaluation of their industrial potentials. In this manuscript, uncalcined MgCoAl, calcined MgCoAl, uncalcined graphene-MgCoAl, and calcined Graphene-MgCoAl are referred to as MCA, MCA-C, G/MCA, and G/MCA-C, respectively.

MATERIALS AND METHOD

1. Materials

Graphene (GRAFEN®-SEG/semi-exfoliated graphene sheets) was procured from GRAFEN future engineering (Ankara, Turkey). Cobalt nitrate hexahydrate [$Ni(NO_3)_2{\cdot}6H_2O$] was purchased from Sigma-Aldrich (USA), while magnesium nitrate hexahydrate [$Mg(NO_3)_2{\cdot}6H_2O$], and aluminium nitrate nonahydrate [$Al(NO_3)_3{\cdot}9H_2O$] were procured from Sigma-Aldrich CO. (Germany). The chemicals procured are highly pure (>97%), so they were used without further purification. Deionized water (DI) was used for solution preparations as well as dilution.

2. Synthesis of Ternary LDH and Graphene/Ternary LDH composite

Nearly 0.04 moles of aluminium salt, 0.04 moles of cobalt salt and 0.08 moles of magnesium salt (to achieve a total M^{2+} to M^{3+} ratio of 3) were dissolved in 80 ml of DI water followed by vigorous stirring at 1,000 rpm in an oil bath at 60 °C for about 15 minutes. Subsequently, 1 M NaOH was added dropwise to stabilize the pH at 10±0.5 while maintaining the stirrer speed and temperature of 60 °C. Thereafter, the temperature was raised to 90 °C and stirring increased to 900 rpm while the reaction was refluxed for 24 hours. The suspension obtained was washed twice with DI H_2O and then twice again using ethanol to remove impurities. The densely-obtained slurry was dried for 24-48 h at 80 °C.

Graphene/ternary LDH composite was synthesized as above with slight modification. Precisely, 300 mg of graphene was added to 60 ml NaOH (0.2 M) and the mixture ultra-sonicated at 60 rpm for 90 min. The obtained mixture was then added to a prepared mixture of the ternary LDH precursor and two to three drops of hydrazine added. Other procedures were followed as outlined in the synthesis of MCA. Both ternary MCA and G/MCA were calcined at 400 °C for 4 h under a 130 mL min^{-1} N_2 environment to produce MCA-C and G/MCA-C, respectively, and stored in glass vials for use in the adsorption experiments.

3. Characterization of MCA, G/MCA, MCA-C, and G/MCA-C

The crystallography via X-Ray diffraction was investigated with the use of a Rigaku MinifeFlex II diffractometer with parameters step-size, scan rate and 2θ range set at 0.03, 3^0/min and 5-70^0, respectively. The FTIR spectra were measured at room temperature on Nicolet 6700 spectrometer. The thermal behavior and decomposition pattern via thermogravimetric analysis was recorded on a TGA/DSC (SDT-Q600) analyzer by heating dry powder at 10 °C/min. The FE-SEM using TIMA TESCAN SEM Integrated system was used to obtain the microstructure of the samples. BET analyzer (Micromeritics, Tristar II series) was used to determine the specific surface area, pore volume, and pore radius.

4. Preparation of the Methyl Orange (MO) Solution

A stock solution of 200 mg/L of MO dye was prepared with 200 mg dissolved in 1 liter of deionized water which was diluted to the required concentrations.

5. MO Adsorption Investigation

The batch mode was carried out by shaking 30 ml of dye solution in 150 ml glass-flask of dye solution on a shaker (Lab Companion SK-600 Benchtop, 120VAC, 60Hz, 0.4A) set at 180 rpm. The influence of the principal adsorption parameters via equilib-

rium and kinetics studies was investigated. The required pH (2-9) of the mixture was obtained using a 0.1 M NaOH or a 0.1 M HNO_3 solution with a HANNA (HI 2211) pH/ORP meter. After agitation, the adsorbent and adsorbate mixture was centrifuged (3,500 rpm for 5 minutes) to allow separation. The final concentration of adsorbate (MO) was calculated from the area under the curve of maximum absorbance (340-580 nm) measured by a Jasco V-670 UV-Visible Spectrometer.

The equilibrium adsorption capacity (q_e), time-dependent adsorption capacity (q_t) and percentage dye removal (%) were computed from the following equations:

$$\% \text{ Dye removal} = \frac{C_o - C_e}{C_o} * 100 \quad (1)$$

$$q_t = \frac{C_o - C_t}{M} * V_S \quad (2)$$

$$q_e = \frac{C_o - C_e}{M} * V_S \quad (3)$$

where C_o, C_e, and C_t, respectively, represent initial, equilibrium and time-dependent dye concentrations (mg/L). M and V_S are the mass of adsorbents (mg) and the volume of dye solution used (mL).

6. Adsorption Isotherms

The equilibrium data were fitted to four common adsorption isotherm models: Langmuir, Freundlich, Redlich-Peterson and Temkin. The Langmuir isotherm is considered accurate on the premise that the adsorption occurred on monolayer surfaces with equivalent energies, no interaction occurred among adsorbed molecules and the same adsorption mechanism is experienced by all molecules [21]. The Langmuir model is given as

$$q_e = \frac{q_m b C_e}{1 + b C_e} \quad (4)$$

where q_m (mg/g) and b (L/mg) are Langmuir constants signifying maximum monolayer adsorption capacity and a parameter relating to the free energy of adsorption, respectively [22]. Linearizing Eq. (4) gives

$$\frac{C_e}{q_e} = \frac{1}{b q_M} + \frac{C_e}{q_m} \quad (5)$$

The values of q_m and b are obtained from the slope and intercept, respectively, of the linear plot of C_e/q_e versus C_e in Eq. (5). Another parameter termed the separation factor, R_L, defined in Chen et al. [23] signifies unfavorable, linear, favorable, and irreversible adsorption for $R_L>1$, $R_L=1$, $0<R_L<1$ and $R_L=0$, respectively.

$$R_L = \frac{1}{1 + b C_o} \quad (6)$$

On the other hand, the Freundlich isotherm assumes multi-layered heterogeneous adsorption with the heat of adsorption distribution [24], and its non-linear and linear forms are given in Eq. (7) and Eq. (8), respectively.

$$q_e = K_F C_e^{1/n} \quad (7)$$

$$\log q_e = \log K_F + \frac{1}{n} \log C_e \quad (8)$$

where n and K_f are Freundlich constants indicating adsorption intensity and distribution coefficient relating to bonding energy respectively [11]. $1/n<1$ indicates a normal Langmuir isotherm while $1/n>1$ is cooperative adsorption [25]. The values of 1/n and K_F are obtained from the slope and intercept, respectively, of the linear plot of $\log q_e$ versus $\log C_e$ in Eq. (8).

Redlich-Peterson (RP) isotherm is a three-parameter model that combines Langmuir and Freundlich isotherms [26] and is defined as

$$\frac{C_e}{q_e} = \frac{B}{A} + \left(\frac{1}{A}\right) C_e^N \quad (9)$$

Parameter N ranges between 0 and 1. A, B and N are obtained by curve fitting.

Temkin isotherm [27] considers the adsorbate-adsorbent interaction where the heat adsorption reduces linearly with coverage for all molecules. In nonlinear and linear forms, it is represented, respectively, as

$$q_e = Y \ln(X C_e) \quad (10a)$$

$$q_e = Y \ln X + Y \ln C_e \quad (10b)$$

and B is defined by

$$Y = RT/b_T \quad (11)$$

$1/b_T$ defines the adsorbent adsorption potential, T (K) is absolute temperature and R is the gas constant.

7. Adsorption Kinetics

To investigate the sorption rate and a suitable reaction mechanism for the new adsorbents, the experimental data were fitted to the linearized forms of the pseudo-first-order (PFO), pseudo-second-order (PSO), Elovich and intra-particle diffusion (IPD) models shown in Eqs. (12), (13), (14) and (15) respectively:

$$\log(q_e - q_t) = \log q_e - \frac{k_1 t}{2.303} \quad (12)$$

$$\frac{t}{q_t} = \frac{1}{k_2 q_e^2} + \frac{t}{q_e} \quad (13)$$

$$q_t = \frac{1}{\beta} \ln(\alpha\beta) + \frac{1}{\beta} \ln(t) \quad (14)$$

$$q_t = k_d t^{1/2} + C \quad (15)$$

where k_1 (min^{-1}) and k_2 (g mg^{-1} min^{-1}) are rate constants from pseudo-first-order and pseudo-second-order models, respectively. α (g mg^{-1} min^{-1}) and β (g mg^{-1}) denote initial adsorption and desorption coefficients, respectively. k_d (g mg^{-1} $min^{-1/2}$) represents the intra-particle diffusion rate constant. All constants are obtained from the linear regression of their respective equations.

RESULTS AND DISCUSSION

1. Characterizations of MCA, G/MCA, MCA-C, and G/MCA-C

LDHs possess unique characteristic diffraction peaks [11,28] which are well established in the ternary LDH as presented in Fig. 1(a). The intensity of the symmetric peak at 11.36° assigned to the (003) plane indicates a well-defined crystalline structure with an associated basal spacing of 0.775 nm. The other peaks at 2θ=

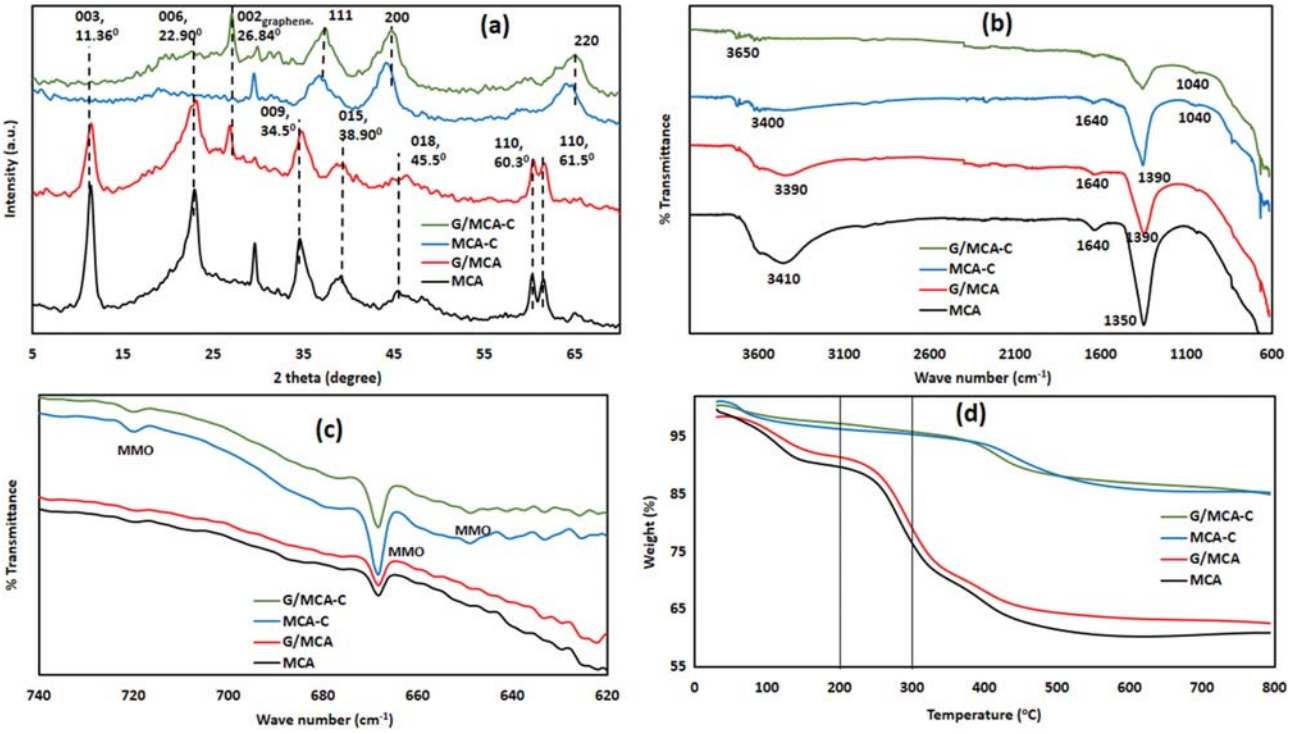

Fig. 1. X-ray diffractions (a), FTIR spectra for high range (b), FTIR spectra for low range (c), Thermogravimetric analysis (d) of MCA, G/MCA, MCA-C, and G/MCA-C.

22.9°, 34.5°, 38.9°, 45.5°, 60.3°, and 61.5° are indexed to the (006), (009, (015), (018), (110) and (113) respective planes. The pristine graphene shows its peak at 26.84° 2θ assigned to the (002) plane [29,30]. The G/MCA maintains a similar structure to MCA due to the occurrence of similar (110) and (113) peak planes [17] but with graphene induced broadness in the (003) and (006) planes of G/MCA. The broadness may be ascribed to the occurrence of electrostatic interaction in the composite which affected the nucleation and crystal size of the LDH [31]. A similar observation has been previously reported [17]. Upon calcination, the LDH peaks become alienated due to the destruction of its structure resulting in the formation of mixed metal oxides (MMO) known with peaks located at the (111), (200) and 220 planes [13,32].

FTIR analysis is an important tool to help understand the active sites and interactions of the group responsible for the adsorption. Fig. 1(b) depicts the FTIR of MCA, G/MCA, MCA-C, and G/MCA-C. For all four spectra, the peaks between 3,400 and 3,600 cm^{-1} are assigned to the stretching modes of the interlayer water molecule, while the bending modes of water are at 1,640 cm^{-1} [33]. The sharp stretched peaks at 1,350 cm^{-1} and 1,390 cm^{-1} in MCA and G/MCA spectra are associated with interlayer anions (NO_3^-) [28]. In addition, calcination led to the removal of the interlayer and physisorbed water molecules and interlayer anions, and this is evident in peak reduction in both MCA-C and G/MCA-C. This further confirms the alteration of the structure of the LDHs as previously established by XRD. After calcination, a new peak at 1,040 cm^{-1} corresponding to C-O-C bond appeared. Likewise, the presence of new peaks below 800 cm^{-1} in both MCA-C and G/MCA-C spectrum (Fig. 1(c)) indicates the abundant formation of mixed metal oxides on graphene sheets. FTIR results clearly suggest that the coupling of graphene and calcination led to significant improvement in surface functionalities of the ternary LDH and may be expected to profoundly increase the MO adsorption capacity [34].

Thermal behavior and temperature dependent decomposition patterns of the synthesized samples were investigated by thermogravimetric analysis (TGA) under nitrogen environment up to 800 °C as shown in Fig. 1(d). MCA and G/MCA experience three modes of weight losses which resulted in total weight reduction by 39% and 37.7%, respectively. Physisorbed and intercalated water molecules are removed up to a temperature below 200 °C in the first stage [3], and this accounts for 10.4 and 8.5% loss. This is subsequently followed by dehydroxylation (DH), decarboxylation (DC) and removal of other interlayer anions such as nitrates in the second stage of weight loss between 200 °C and 400 °C, which resulted in 23.3% loss for both. The third stage involves little weight beyond 400 °C with further decarboxylation and dehydroxylation results in the production of mixed metal oxides (MMO) as confirmed from FTIR analysis [35]. MCA-C and G/MCA-C experience two modes of weight reduction which are mainly due to decarboxylation and the interlayer anions removal and formation of MMO. Most of the water molecules have been eliminated due to calcination. Between (35 °C and 40 °C), both MCA-C and G/MCA-C gained weight due to absorption of water molecules from the environment, and these were subsequently removed with an increase in temperature.

The BET surface areas, pore volumes and average pore sizes of MCA, G/MCA, MCA-C, and G/MCA-C obtained using N_2 adsorption and desorption isotherms are listed in Table 1. The nitro-

Table 1. Surface area, pore size and pore volume of the MCA and G/MCA composites

Sample	Surface area (m^2/g)	Pore size (A)	Pore volume (cm^3/g)
MCA	122.5050	15.5200	0.1906
G/MCA	163.2780	17.7800	0.0944
MCA-C	142.9910	82.2000	0.1708
G/MCA-C	268.2240	16.0700	0.0671

gen adsorption-desorption isotherm in Fig. S1 (supplementary data) shows a type IV isotherm characteristic of mesoporous materials. The adsorbent materials are characterized by high surface areas, which are significant for adsorption. It is apparent that the surface area of MCA, 122.5 m^2/g, was increased by the introduction of graphene to 163.3 m^2/g and by calcination to 143.0 m^2/g corresponding to an increment of 33.3% and 16.7%, respectively. Due to the synergistic contribution of both calcination and graphene introduction, G/MCA-C possesses the highest surface area of 268.2 m^2/g. Additionally, there is a reduction of the pore size and the pore volume from 17.78 A to 16.07 A and 0.0944 cm^3/g to 0.0671 cm^3/g of G/MCA after calcination. Such synergistic contributions have been previously reported with respect to Cr(IV) removal by calcined G-MgAl LDH [19]. Thus, G/MCA-C is expected to have profound uptake of MO anions, which can make potentially a superb sorbent material for treatment of dye-contaminated wastewater.

The SEM microstructures images of the adsorbent samples are shown in Fig. 2(a)-(d). The SEM of MCA (Fig. 2(a)) shows a large number of loose flower-like nanoparticles which are uniformly distributed. The morphology observed is a result of the synthesis route which has previously been reported [36]. Introduction of graphene to form G/MCA (Fig. 2(b)) resulted in the formation of irregularly shaped plate-like nanosheets with overlapping configuration. The calcination resulted in the formation of the adsorbents with rough and compact surfaces. The TEM images in Fig. 2(e)-(f) show strong evidence of nanosheet-like morphology of G/MCA with homogeneous dispersion of graphene on the plate-like LDH. The homogeneous dispersion of the graphene contributed to the observed higher surface area of G/MCA.

2. Adsorption Parameters

2-1. Effect of Initial pH

The surface charge, active sites dissociation of the functional group of the adsorbent, extent of ionization and structure of the dye molecules are predominantly affected by pH [22,37]. The percentage of dye removal dependence on pH when the pH was varied from 3 to 9 is shown in Fig. 3(a); meanwhile, Fig. S2 (supplementary data) displays the point of zero charges (pH_{PZC}) of MCA, G/MCA, MCA-C and G/MCA-C determined by the pH drift method [38]. The pH_{PZC} of MCA, G/MCA, MCA-C, and G/MCA-C are 4.99, 5.17, 5.94 and 5.94, respectively. The MO percentage removal was observed to decline for a rise in pH from 3 to 9, and this trend is experienced by all the adsorbents. Similar behaviors were associated with other LDHs as reported elsewhere [3].

Surface charges of the adsorbents in the aqueous medium can be used to substantiate these behaviors. For pH 3 below the pH_{PZC}, the adsorbents possess a positively charged surface (protonated), which enhances electrostatic attraction to negatively charged molecules of the anionic dyes. Hence, the highest removal of the dye of 83%, 88%, 96% and 98% for MCA, G/MCA, MCA-C, and G/MCA-C, respectively, was achieved at pH 3. The highest percent-

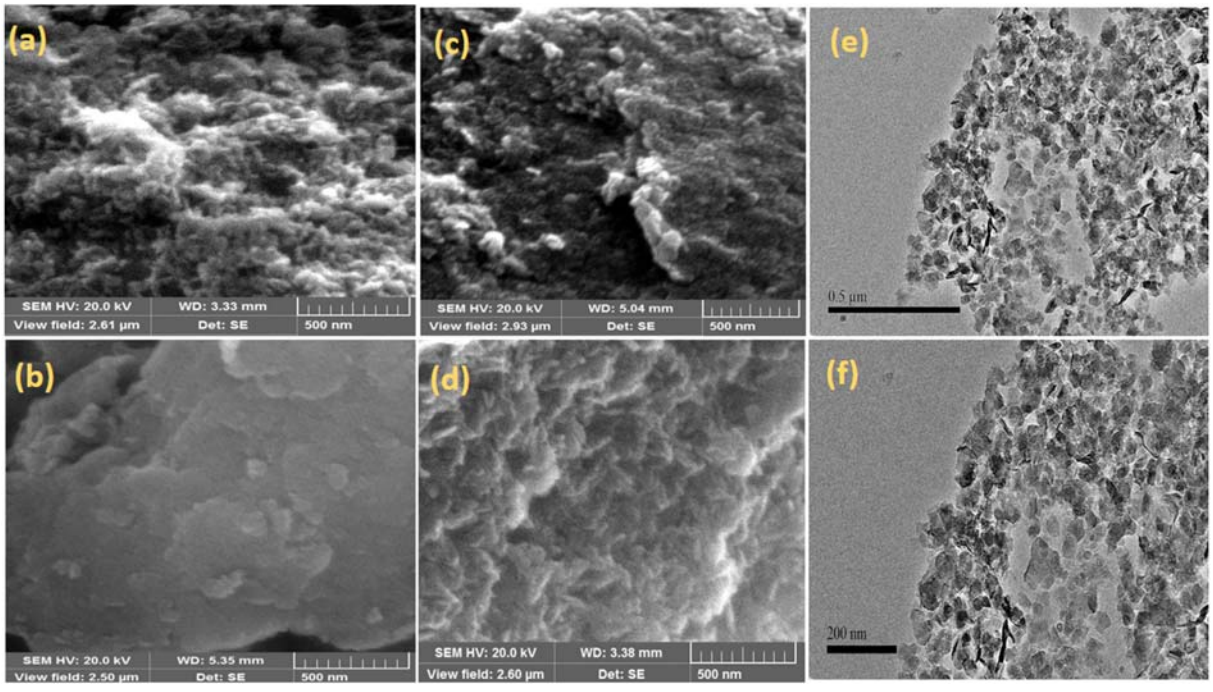

Fig. 2. SEM of MCA (a), G/MCA (b), MCA-C (c), G/MCA-C (d) G/NMA; TEM images of G/MCA at low magnification (e), high magnification (f).

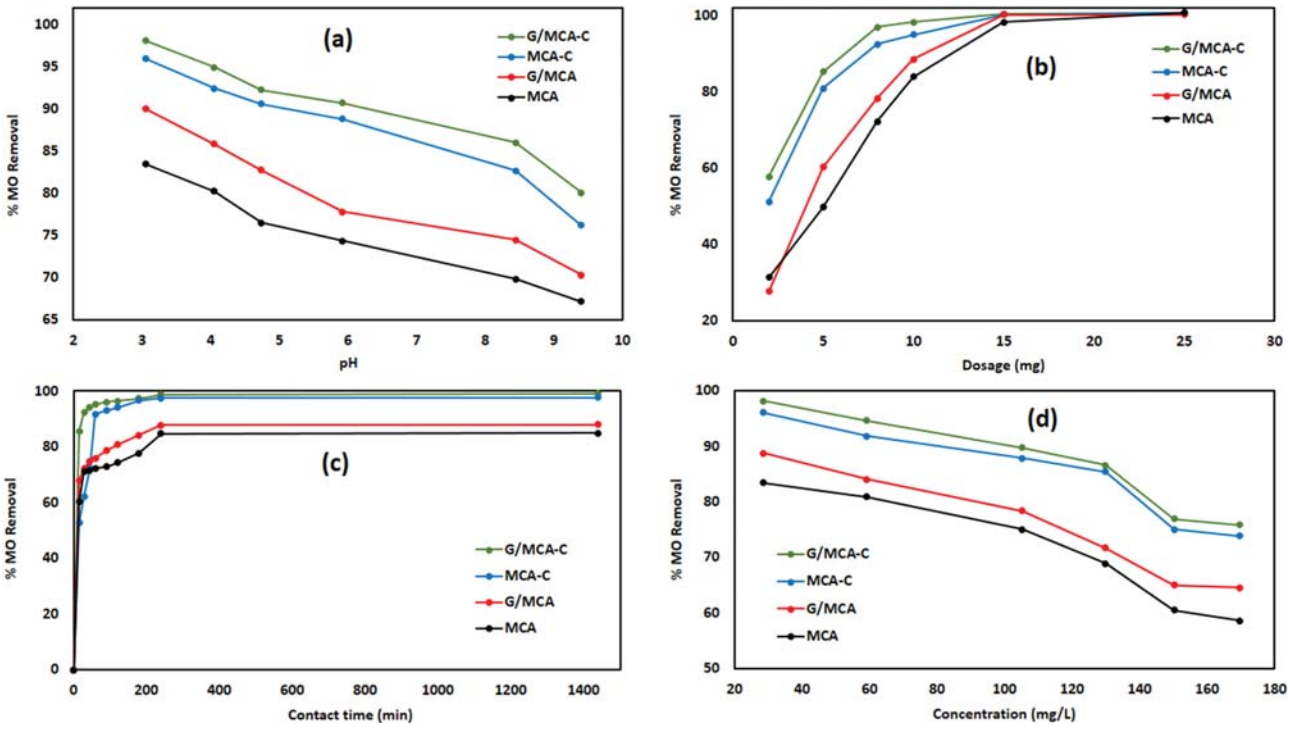

Fig. 3. Effects of (a) pH at C_0=30 mgL^{-1}, adsorbent dosage=10 mg and contact time=180 min (b) dosage at pH=3, C_0=30 mgL^{-1} and contact time=180 min (c) contact time at pH=3, C_0=30 mgL^{-1} and adsorbent dosage=10 mg (d) concentration at pH=3, adsorbent dosage=10 mg and contact time=180 min.

age removal of G/MCA-C compared to other adsorbents is associated to the increase in specific surface area and presence of MMO on its surface as confirmed from BET and FTIR providing higher active binding sites for uptake of MO. As the pH was increased to pH 4 and above, there was a reduction in the number of positively-charged adsorption sites leading to decreased removal of MO molecules. Furthermore, increasing the pH beyond pH_{PZC} led to the formation of a negatively charged adsorption surface, which stimulates electrostatic repulsion between the anionic dye molecules and adsorbents. However, at a higher pH (>>pH_{PZC}), increased competition between dye molecules and OH^- in aqueous solution in addition to electrostatic repulsion profoundly reduced the percentage dye removal [39]. Consequently, pH 3 was used for the subsequent adsorption studies presented below.

2-2. Effect of Dosage

The variability of percentage MO removal when MCA, MCA-C, G/MCA, and G/MCA-C dosages were varied from 2 mg to 25 mg is shown in Fig. 3(b). The percentage removal increases with increase in adsorbent dosage for all the adsorbents. The percentage removal increased from 28%, 31%, 51%, and 57% to 72%, 78%, 92%, and 96% for a change in dosage from 2 mg to 8 mg for MCA, MCA-C, G/MCA, and G/MCA-C, respectively. These increments can be ascribed to increased supply of active adsorption sites. The highest adsorption was experienced by G/MCA-C, clearly signifying that the addition of graphene onto layers of ternary LDH with subsequent calcination significantly improved active binding sites on the surface. Beyond 10 mg, there was a differential change in percentage removal of the MO with dosage, which indicates the satiation of the quantity of MO molecules by the increased active adsorption sites. Thus, 10 mg was selected as the optimum dosage and was used for subsequent experimentation.

2-3. Effect of Contact Time

The influence of contact time varied from 15 minutes to 1,440 minutes on percentage removal of MO for all the MCA, G/MCA, MCA-C, and G/MCA-C is shown in Fig. 3(c). All four adsorbents exhibited fast sorption in the first 15 minutes with measured removal efficiency of 60, 67, 57 and 85% for MCA, G/MCA, MCA-C, and G/MCA-C, respectively. The MO removal increased with higher contact time until equilibrium was established at 240, 240, 180 and 180 minutes for MCA, G/MCA, MCA-C, and G/MCA-C, respectively. The fast adsorption of calcined samples in the first few minutes can also be attributed to memory effect [19]. The higher adsorption of G/MCA over MCA can be ascribed to the contribution of graphene, which improved the surface area of the nanostructured G/MCA. However, the higher adsorption of MCA-C over MCA was attributed to calcination, which enhances the availability of oxygen-carrying functional groups. Thus, the existence of graphene as a substrate onto layers of ternary LDH with consequent calcination resulted in significant improvement in specific surface area and oxygen functionalities, which tends to the fastest and highest adsorption of MO dye molecules experienced by the G/MCA-C [3]. Similar behavior has been reported by Xiaoya Yuan et al. when utilizing calcined graphene-MgAl-LDH for chromium sorption [19].

2-4. Effect of initial MO Concentration

Influence of initial dye concentration on percentage removal of

Table 2. Parameters of isotherm models for adsorption of MO onto MCA and G/MCA composites

Sample	T (K)	Langmuir				Freundlich		
		q_m (mg/g)	K_L	R_L	R^2	K_F	1/n	R^2
MCA	298	357.1400	0.0574	0.0932	0.9930	35.7026	0.5190	0.9423
	308	312.5000	0.0617	0.0873	0.9838	34.1350	0.4958	0.9041
	318	208.3300	0.1237	0.0455	0.9720	38.6634	0.3841	0.7828
G/MCA	298	384.6200	0.0695	0.0782	0.9958	45.2585	0.4908	0.9714
	308	344.8300	0.0673	0.0806	0.9936	40.1051	0.4872	0.9374
	318	256.4100	0.0958	0.0580	0.9767	39.6552	0.4282	0.8213
MCA-C	298	400.0000	0.1724	0.0331	0.9944	81.6770	0.4190	0.9627
	308	384.6200	0.1970	0.0291	0.9829	62.1727	0.4805	0.9444
	318	357.1400	0.0841	0.0655	0.9928	46.7951	0.4768	0.9198
G/MCA-C	298	434.7800	0.1345	0.0420	0.9783	106.6596	0.3570	0.9771
	308	400.0000	0.1689	0.0337	0.9973	77.9292	0.4328	0.9246
	318	370.3700	0.0957	0.0580	0.9961	52.7715	0.4655	0.9347
		Redlich-peterson				Temkin		
		A	B	N	R^2	X	Y	R^2
MCA	298	330.9000	15.7151	0.9816	0.9921	0.5120	82.6580	0.9810
	308	218.7200	9.81850	0.9243	0.9779	0.5150	73.6910	0.9416
	318	137.2600	0.00620	0.9267	0.9433	0.9000	47.3530	0.7595
G/MCA	298	319.5900	11.2624	0.9584	0.9959	0.7080	83.2070	0.9888
	308	314.9600	13.1499	0.9824	0.9929	0.6190	77.5630	0.9709
	318	204.8100	7.1832	0.9522	0.9724	0.7540	59.5450	0.8365
MCA-C	298	347.7700	4.6280	0.9633	0.9945	2.1450	79.9170	0.9681
	308	338.3100	6.5641	0.9542	0.9958	1.1280	90.3020	0.9833
	318	229.0700	6.2138	0.9011	0.9958	0.7660	79.9770	0.9650
G/MCA-C	298	251.8500	1.5027	0.8842	0.9972	4.9130	69.3830	0.9772
	308	370.3000	5.2611	0.9801	0.9971	1.8130	83.3980	0.9739
	318	283.8400	7.1214	0.9422	0.9941	0.9180	80.8500	0.9765

MO is depicted in Fig. 3(d). The plot shows that there was a reduction in percentage removal as initial concentration was increased. When the MO concentration was increased at a fixed adsorbent dosage, active sites were also fixed in number, were occupied and free active binding sites were continuously filled up. Hence, unadsorbed dye molecules were left in the solution after the complete occupation of adsorption sites. At 30 mg/L MO concentration, the percentage removal of MO of 83%, 88%, 96% and 98% significantly, decreased to 60%, 65%, 75% and 77% when the concentration was increased to 150 mg/L for MCA, G/MCA, MCA-C, and G/MCA-C, respectively, for a fixed dosage of 10 mg for a contact time of 180 min. Further increases in the MO concentration induced more reduction in the MO percentage removal. As previously observed, G/MCA-C experienced the highest adsorption of all initial MO concentrations due to the synergistic interplay previously explained.

3. Isotherm Studies

An adsorption isotherm study is significant in designing an adsorption system due to its importance in estimating the adsorbent adsorption capacity as well as analyzing the interaction between adsorbate and adsorbent at equilibrium [40]. Thus, equilibrium data were applied to Langmuir, Freundlich, Temkin, and Redlich-Peterson isotherm models via linear regression technique. The values of the various parameters and correlation coefficients are summarized in Table 2 and their linear plots displayed in Fig. 4(a)-(d). The isotherm results showed that at all temperatures (298-318) K, Langmuir and Redlich Peterson models adequately fit the experimental data with the higher correlation coefficients (R^2>0.98) in comparison to Freundlich and Temkin isotherm models. Thus, the sorption of methyl orange molecules onto four sorbents took place in both homogeneous and heterogeneous manner. The equilibrium constant K_L value of G/MCA-C (0.1345) was higher than that of MCA (0.0574) and G/MCA (0.0695), which means stronger affinity between MO and sorbent G/MCA-C. In addition, the values of R_L ($0<R_L<1$) (Table 2) further confirmed the favorability of the adsorption process for all the four adsorbents. The maximum adsorption capacity at 298 K was 357.14 mg/g, 384.62 mg/g, 400 mg/g and 434.78 mg/g for MCA, G/MCA, MCA-C and G/MCA-C, respectively. Higher sorption values of G/MCA-C compared to other adsorbents demonstrated to a large extent that modified with graphene and calcination could enhance the adsorption performance of MCA ternary LDH noticeably. The decrease in maximum adsorption capacity of all adsorbents with an increase in temperature from 298 K to 318 K indicates the unfavorability of

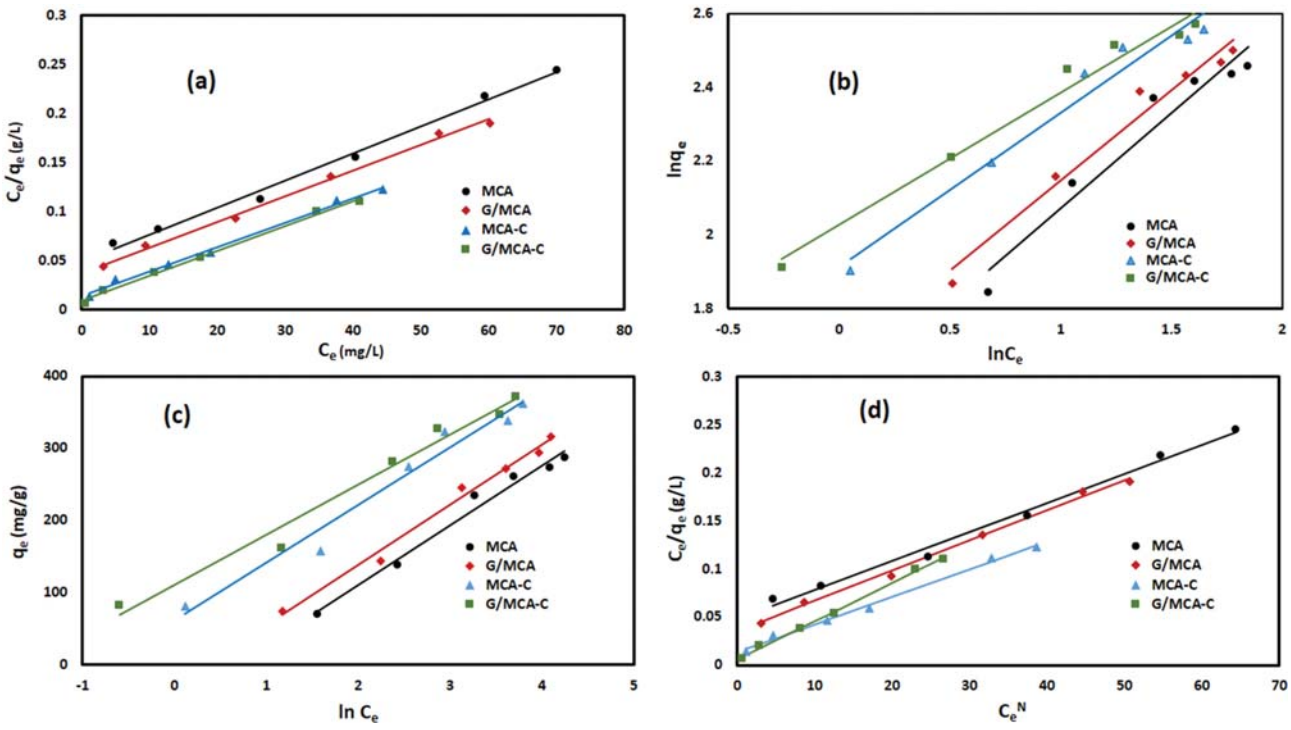

Fig. 4. (a) Langmuir (b) Freundlich (c) Temkin isotherm models and (d) Redlich-peterson isotherm models for MCA, G/MCA, MCA-C and G/MCA-C at 298 K.

Table 3. Parameters of kinetic models for adsorption of MO onto MCA and G/MCA composites

Adsorbent		PFO			PSO		
	$q_{e\,(exp)}$	$q_{e(cal)}$	k_1	R^2	$q_{e(cal)}$	$k_2 * 10^{-2}$	R^2
MCA	89.7450	39.1832	0.0164	0.7221	90.0901	0.1101	0.9943
G/MCA	92.8870	35.1480	0.0168	0.8621	94.3396	0.1186	0.9983
MCA-C	103.0710	62.9360	0.0256	0.9596	111.1111	0.0593	0.9972
G/MCA-C	104.6070	12.7790	0.0145	0.8921	105.2630	0.3432	0.9999
		Elovich			IPD		
	$q_{e\,(exp)}$	α	β	R^2	C	k_d	R^2
MCA	89.7450	4645.4100	0.1387	0.8560	62.0040	1.6652	0.8355
G/MCA	92.8870	8952.3500	0.1384	0.9834	66.6410	1.6933	0.9880
MCA-C	103.0710	29.2300	0.0539	0.8711	50.4700	4.0186	0.7472
G/MCA-C	104.6070	6.0390 E8	0.2305	0.8706	91.2670	0.9310	0.7330

the adsorption at higher temperatures.

4. Kinetic Studies

The kinetic parameters of pseudo-first order, pseudo-second order, Elovich, and intra-particle diffusion models are listed in Table 3 and the linear plots shown in Fig. 5(a)-(d). From the tabulated result, it is deduced that the pseudo-second-order model adequately fits the experimental data with the highest correlation coefficient (R^2>0.99). Also, the maximum adsorption capacity from the pseudo-second-order model closely matches the experimental value. It can be stated that the rate controlling mechanism of the adsorption is dominated by chemisorption, which is the basic assumption the pseudo-second-order model was built on [41]. Similar results have been published indicating chemisorption as the controlling step in the removal of many dyes by LDHs [3,36,42,43]. Furthermore, the intra-particle diffusion kinetic model was employed to evaluate the actual rate determining steps (Fig. 5(d)). According to the linearization of the intra-particle diffusion plot, two and three main steps were dominated by MO sorption process for uncalcined and calcined composites, respectively. The first step includes fast sorption rate and is associated with the surface adsorption phenomena onto active binding sites on the adsorbent external surface. The second step is attributed to the inclusion of MO anions into the pores of composites and the third is the equilibrium step indicating saturation of binding sites [44].

5. Thermodynamics and Effect of Temperature

The effect of temperature and change in internal energy relat-

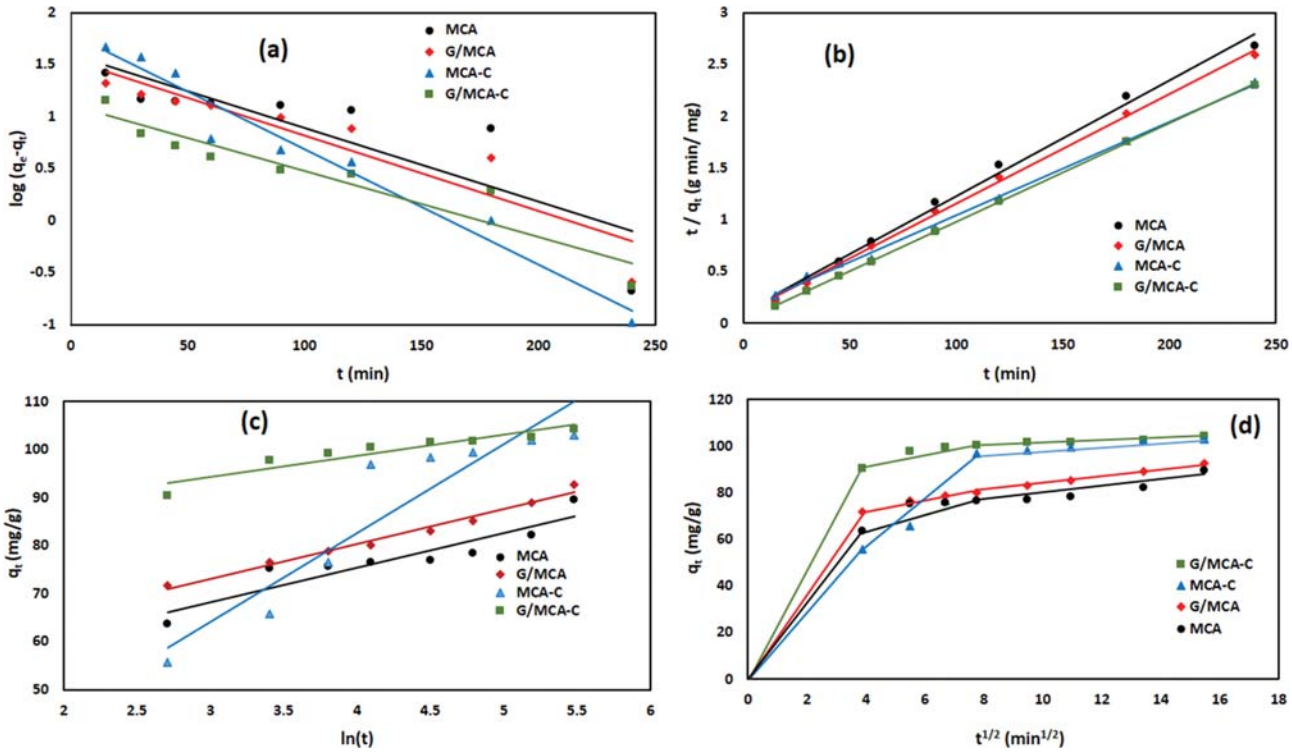

Fig. 5. (a) Pseudo first order (b) pseudo second order (c) elovich (d) intra-particle diffusion models for MCA, G/MCA, MCA-C and G/MCA-C at 298 K.

ing to adsorption processes are important and they can be provided from thermodynamic consideration through changes in enthalpy (ΔH), Gibb's free energy (ΔG) and entropy (ΔS) according to the following relationship,

$$\Delta G = -RT\ln K_D \quad (16)$$

$$\ln K_D = \frac{\Delta S}{R} - \frac{\Delta H}{RT} \quad (17)$$

where R (8.314 J/mol/K) is the molar gas constant and T (K) is the absolute temperature (K). K_D (L/g) is a thermodynamic equilibrium constant obtained by plotting $\ln(q_e/C_e)$ versus q_e and extrapolating q_e to zero [45]. ΔG is estimated from Eq. (16), while ΔH and ΔS are computed from the slope and intercept of the linear plot of $\ln K_D$ versus 1/T in Eq. (17). In this study, three temperatures (298 K, 308 K, and 318 K) were considered to estimate the thermodynamic parameters. The values of the thermodynamic parameters are presented in Table 4 and the linear graph of $\ln K_D$ versus 1/T is shown in Fig. 6.

Thus, these results indicate that the adsorption of MO by all the tested adsorbents is characterized by feasibility and spontaneity (negative ΔG) and is exothermic (negative ΔH). This implies a decrease in adsorption and reduced spontaneity with increases in temperature as further suggested by the decreasing K_d being in agree-

Table 4. Thermodynamic parameters for adsorption of MO on MCA and G/MCA composites at 298-318 K

Sample	T (k)	K_d	ΔG	ΔH	ΔS
MCA	298	3.200	−2.882	−5.362	−8.281
	308	3.028	−2.837		
	318	2.792	−2.714		
G/MCA	298	3.615	−3.184	−7.181	−13.355
	308	3.360	−3.103		
	318	3.011	−2.914		
MCA-C	298	4.761	−3.866	−11.059	−24.124
	308	4.141	−3.639		
	318	3.595	−3.383		
G/MCA-C	298	5.649	−4.290	−15.179	−36.559
	308	4.600	−3.908		
	318	3.843	−3.559		

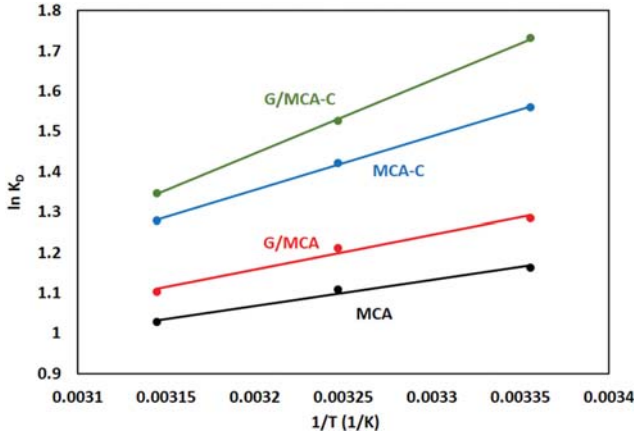

Fig. 6. Linear plot of $\ln K_D$.

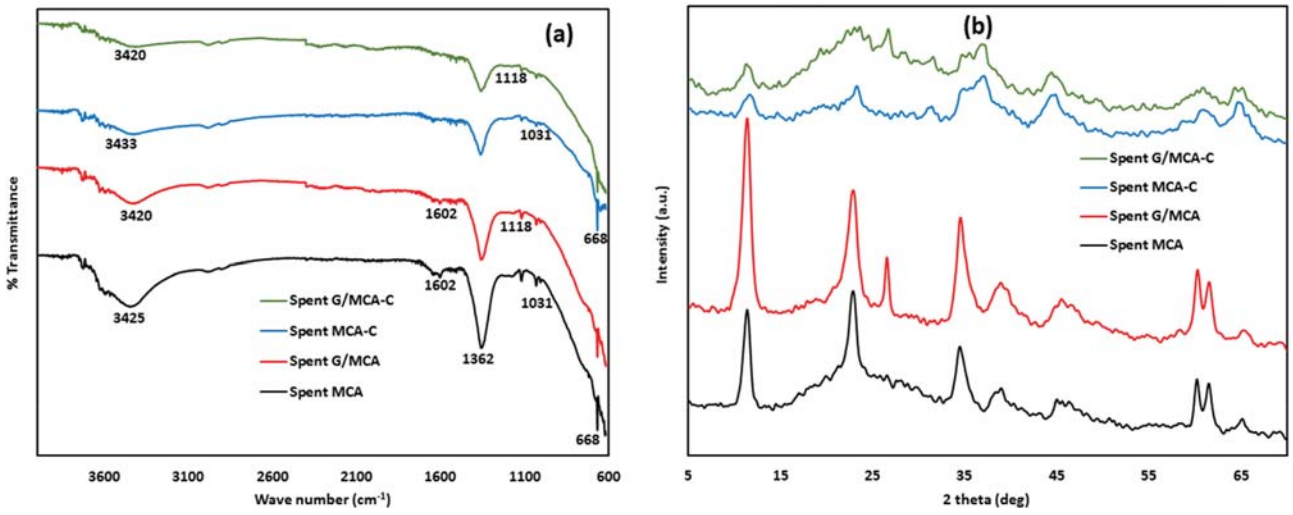

Fig. 7. (a) FTIR (b) XRD of spent MCA, G/MCA, MCA-C and G/MCA-C.

ment with increasing ΔG with increasing temperature [45,46]. The negative values of ΔS for the four samples are an indication of reduced randomness at the absorbate/adsorbent interface and greater order of reaction associated with adherence of the dye on the surface of the adsorbents with a resultant reduction of the system's degree of freedom [47,48].

6. Adsorption Mechanism

FTIR and XRD analyses of the spent MCA, G/MCA, MCA-C, and G/MCA-C adsorbents were undertaken to understand the interaction of active sites on the adsorbent and functional groups of the dyes which can help better understand the adsorption mechanism [49,50]. From the FTIR results obtained as shown in Fig. 7(a), it is obvious that new peaks appeared after the MO adsorption on all the adsorbents. A new band at 1,118 cm^{-1} corresponds to the C-N bond vibration, while the band at 1,031 cm^{-1} is ascribed to the symmetric stretching vibration of the -SO_3^- of the MO [49,51, 52]. This suggests that molecules of the MO dye are effectively fastened on the surfaces of the adsorbents via electrostatic and chemical interactions. The peak of the NO_3^- vibration located at 1,350 cm^{-1} on fresh adsorbents weakened and slightly shifted to a higher wavenumber on the spent adsorbents, suggesting chemical interaction. The reduction of peaks' intensities at 3,400-3,600 cm^{-1} and below 800 cm^{-1} attributed to the stretching and bending modes of interlayer water molecules and mixed metal oxides, respectively, further demonstrated that there was a substantial contribution of chemical bonding in the MO-G/MCA-C adsorption system [53].

Fig. 7(b) shows the XRD of all the four spent adsorbents. Noticeably, no significant changes were observed in the peak positions of MCA and G/MCA except the changes related to diffractogram peak intensities, indicating more random crystal deformation [50,54]. This suggested that anion surface adsorption is one of the mechanisms of adsorption as proposed by Wang and group [55]. The spent MCA-C and G/MCA-C were reconstructed via a memory effect to their respective LDHs. It can be construed that intercalation via reconstruction and rehydration plays an important role in the adsorption of the MO on the surfaces of the MCA-C and G/MCA-C [38]. Hence, the proposed mechanisms of adsorption for MCA and G/MCA include electrostatic interactions, surface adsorption, and hydrogen bonding, while surface reconstruction along with ion exchange, electrostatic interactions and strong chemical bonding between MO anions and surface oxygen functionalities are involved for MCA-C and G/MCA-C. Moreover, hybridization of MCA LDH crystals with graphene and calcination led to significant enhancement in surface area and oxygen functionalities, providing more active binding sites for MO.

7. Regeneration and Reuse of Adsorbents

Economic feasibility of an adsorption process is highly influenced by adsorbent regeneration and reuse potentials which could account for saving of up to 70% of the operation and maintenance costs [56,57]. To regenerate the adsorbents tested in this study, 0.1 M NaOH slurries of the spent adsorbents were agitated continuously for 24 hours, filtered and washed several times with deionized water. This treatment was used for subsequent regeneration and reuse applications for the three investigated adsorption cycles. Fig. 8 shows the percentage of MO removal for the three adsorption cycles. The percentage removal decreased from 82, 86, 96 and 99% to 80, 84, 88 and 90% on the second use for MCA, G/MCA, MCA-C, and G/MCA-C, respectively. However, the third reuse showed lit-

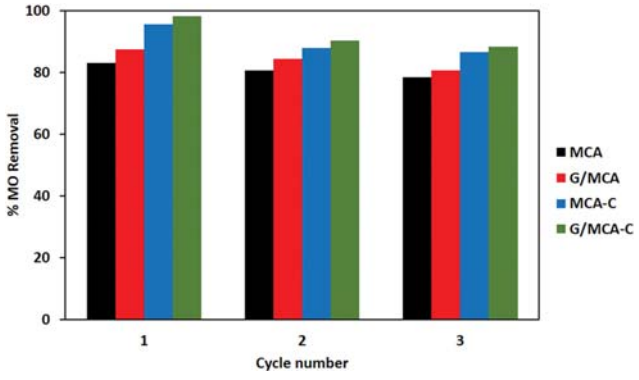

Fig. 8. Percentage removal of MO dye adsorbents after three regeneration cycles.

Table 5. Comparison of adsorption capacities of LDHs for MO adsorption

Adsorbent	q_m (mg/g)	References
MgNiAl LDH	375	[11]
Glycerine-MgAl LDH	443.5	[49]
Biomorphic MgAl MMO	182.8	[32]
Fe_3O_4/ZnCr	240.16	[58]
MgAl	148	[59]
ZnAl-LDO	181.9	[60]
NiFe	246.91	[3]
Starch-NiFe	387.59	[3]
MCA	357.14	This work
G/MCA	384.62	This work
MCA-C	400.00	This work
G/MCA-C	434.78	This work

tle reduction in the removal efficiency to 78, 81, 87, and 88%, respectively. This clearly indicates that all the adsorbents employed in this study are characterized by high regeneration and reusability potentials, thereby, showcasing their potential for cost-effective deployment in the treatment of real water and wastewater for removal of dyes.

8. Comparison to Other Adsorbents

The performance of the MCA, G/MCA, MCA-C, and G/MCA-C adsorbents in terms of the maximum achievable adsorption capacity was compared with other LDHs reported in the literature as highlighted in Table 5. These tested adsorbent materials perform better than most of the similar reported LDHs, which buttresses their huge potential in water treatment applications.

CONCLUSION

This study reports the synthesis via co-precipitation of ternary LDH, MCA, and its graphene nanocomposite, G/MCA and heat treatment through calcination at 400 °C for 3 hours for the removal of methyl orange from aqueous phase. Characterization of the hybrid materials reveals homogeneously dispersed graphene on the LDH leading to substantial improvement in surface area and formation of oxygen functionalities after calcination, which contributed immensely to the fast and effective MO removal from the water phase. For all adsorbents, the adsorption parametric study reveals that the optimal condition occurred at pH and 10 mg dosage, while equilibrium was established at 180 and 240 min for G/MCA-C and MCA, respectively. Isotherm study shows the suitability of Langmuir and Redlich Peterson isotherms models with maximum adsorption capacity of 357.14 mg/g, 384.62 mg/g, 400.00 mg/g and 434.78 mg/g for MCA, G/MCA, MCA-C, and G/MCA-C, respectively. Kinetics study demonstrated well by the pseudo-second-order model. Thermodynamic studies show the spontaneous and exothermic nature of the adsorption with lower adsorption at higher temperature. The characterization (FTIR and XRD) of spent adsorbents demonstrated that the sorption mechanism of MO molecules is controlled by surface adsorption and strong electrostatic and chemical interactions. The adsorbents with their better surface properties and adsorption performance coupled high reusability demonstrate their potential as efficient materials for water treatment.

ACKNOWLEDGEMENTS

The authors acknowledge the Center of Research Excellence in Nanotechnology (CENT), Center for Engineering Research (CER) and the department of Chemical Engineering at KFUPM for their huge supports toward the completion of this work.

SUPPORTING INFORMATION

Additional information as noted in the text. This information is available via the Internet at http://www.springer.com/chemistry/journal/11814.

REFERENCES

1. N. I. Blaisi, M. Zubair, Ihsanullah, S. Ali, T. S. Kazeem, M. S. Manzar, W. Al-Kutti and M. A. Al Harthi, *Environ. Sci. Pollut. Res.*, **25**, 34319 (2018).
2. F. P. Sejie and M. S. Nadiye-Tabbiruka, *Phys. Chem.*, **6**, 39 (2016).
3. M. Zubair, N. Jarrah, Ihsanullah, A. Khalid, M. S. Manzar, T. S. Kazeem and M. A. Al-Harthi, *J. Mol. Liq.*, **249**, 254 (2018).
4. F. Harrelkas, A. Azizi, A. Yaacoubi, A. Benhammou and M. N. Pons, *Desalination*, **235**, 330 (2009).
5. E. Bulut, M. Özacar and İ. A. Şengil, *J. Hazard. Mater.*, **154**, 613 (2008).
6. A. Uygur, *Coloration Technol.*, **117**, 111 (2001).
7. M. Liu, Q. Chen, K. Lu, W. Huang, Z. Lü, C. Zhou, S. Yu and C. Gao, *Sep. Purif. Technol*, **173**, 135 (2017).
8. O. Ozdemir, B. Armagan, M. Turan and M. S. Çelik, *Dyes Pigm.*, **62**, 49 (2004).
9. M. D. G. de Luna, E. D. Flores, D. A. D. Genuino, C. M. Futalan and M.-W. Wan, *J. Taiwan Inst. Chem. Engineers*, **44**, 646 (2013).
10. M. Zubair, M. Daud, G. McKay, F. Shehzad and M. A. Al-Harthi, *Appl. Clay Sci.*, **143**, 279 (2017).
11. H. Zaghouane-Boudiaf, M. Boutahala and L. Arab, *Chem. Eng. J.*, **187**, 142 (2012).
12. D. Bharali and R. C. Deka, *Colloids Surf., A: Physicochem. Eng. Aspects*, **525**, 64 (2017).
13. C. Lei, X. Zhu, B. Zhu, C. Jiang, Y. Le and J. Yu, *J. Hazard. Mater.*, **321**, 801 (2017).
14. D. R. Cooper, B. D'Anjou, N. Ghattamaneni, B. Harack, M. Hilke, A. Horth, N. Majlis, M. Massicotte, L. Vandsburger, E. Whiteway and V. Yu, *ISRN Condensed Matter Phys.*, 1 (2012).
15. M. Daud, M. S. Kamal, F. Shehzad and M. A. Al-Harthi, *Carbon*, **104**, 241 (2016).
16. Y. Li, Q. Du, T. Liu, X. Peng, J. Wang, J. Sun, Y. Wang, S. Wu, Z. Wang, Y. Xia and L. Xia, *Chem. Eng. Res. Des.*, **91**, 361 (2013).
17. M. G. Álvarez, D. Tichit, F. Medina and J. Llorca, *Appl. Surf. Sci.*, **396**, 821 (2017).
18. Y. Cao, G. Li and X. Li, *Chem. Eng. J.*, **292**, 207 (2016).
19. X. Yuan, Y. Wang, J. Wang, C. Zhou, Q. Tang and X. Rao, *Chem. Eng. J.*, **221**, 204 (2013).
20. X. Ruan, Y. Chen, H. Chen, G. Qian and R. L. Frost, *Chem. Eng. J.*,

297, 295 (2016).
21. Y. X. Zhang, X. D. Hao, M. Kuang, H. Zhao and Z. Q. Wen, *Appl. Surf. Sci.*, **283**, 505 (2013).
22. R. Lafi, K. Charradi, M. A. Djebbi, A. B. H. Amara and A. Hafiane, *Adv. Powder Technol.*, **27**, 232 (2016).
23. H. Chen, J. Zhao, J. Wu and G. Dai, *J. Hazard. Mater.*, **192**, 246 (2011).
24. P. Monash and G. Pugazhenthi, *Environ. Prog. Sust. Energy*, **33**, 154 (2014).
25. J. Ma, F. Yu, L. Zhou, L. Jin, M. Yang, J. Luan, Y. Tang, H. Fan, Z. Yuan and J. Chen, *ACS Appl. Mater. Interfaces*, **4**, 5749 (2012).
26. O. Redlich and D. L. Peterson, *J. Phys. Chem.*, **63**, 1024 (1959).
27. R. Zandipak and S. Sobhanardakani, *Desalination Water Treatment*, **57**, 11348 (2016).
28. S. Tang and H. K. Lee, *Anal. Chem.*, **85**, 7426 (2013).
29. S. Roy, S. K. Srivastava, J. Pionteck and V. Mittal, *Macromol. Mater. Eng.*, **300**, 346 (2015).
30. D. Iruretagoyena Ferrer, in *Supported Layered Double Hydroxides as CO2 Adsorbents for Sorption-enhanced H2 Production*, Springer International Publishing, Cham, 85 (2016).
31. A. Garcia-Gallastegui, D. Iruretagoyena, V. Gouvea, M. Mokhtar, A. M. Asiri, S. N. Basahel, S. A. Al-Thabaiti, A. O. Alyoubi, D. Chadwick and M. S. P. Shaffer, *Chem. Mater.*, **24**, 4531 (2012).
32. L. Gao, Q. Li, X. Hu, X. Wang, H. Song, L. Yan and H. Xiao, *Appl. Clay Sci.*, **126**, 299 (2016).
33. S. Mallakpour and M. Dinari, *J. Therm. Anal. Calorim.*, **119**, 1905 (2015).
34. S. Yang, L. Wang, X. Zhang, W. Yang and G. Song, *Chem. Eng. J.*, **275**, 315 (2015).
35. D. Chebli, A. Bouguettoucha, A. Reffas, C. Tiar, M. Boutahala, H. Gulyas and A. Amrane, *Desalination Water Treatment*, **57**, 22061 (2016).
36. K. El Hassani, B. H. Beakou, D. Kalnina, E. Oukani and A. Anouar, *Appl. Clay Sci.*, **140**, 124 (2017).
37. J. Liu, X. Li, J. Luo, C. Duan, H. Hu and G. Qian, *Chem. Eng. J.*, **242**, 187 (2014).
38. S. M. Sumari, Z. Hamzah and N. Kantasamy, *Malaysian J. Anal. Sci.*, **20**, 777 (2016).
39. K.-H. Goh, T.-T. Lim and Z. Dong, *Water Res.*, **42**, 1343 (2008).
40. L. Deng, Z. Shi, X. Peng and S. Zhou, *J. Alloys Compd.*, **688**, 101 (2016).
41. Y. S. Ho and G. McKay, *Process Biochem.*, **34**, 451 (1999).
42. Y. Lu, B. Jiang, L. Fang, F. Ling, J. Gao, F. Wu and X. Zhang, *Chemosphere*, **152**, 415 (2016).
43. R.-r. Shan, L.-g. Yan, Y.-m. Yang, K. Yang, S.-j. Yu, H.-q. Yu, B.-c. Zhu and B. Du, *J. Ind. Eng. Chem.*, **21**, 561 (2015).
44. F.-C. Wu, R.-L. Tseng and R.-S. Juang, *Chem. Eng. J.*, **153**, 1 (2009).
45. X. Xin, W. Si, Z. Yao, R. Feng, B. Du, L. Yan and Q. Wei, *J. Colloid Interface Sci.*, **359**, 499 (2011).
46. M. Zubair, N. Jarrah, M. S. Manzar, M. Al-Harthi, M. Daud, N. D. Mu'azu and S. A. Haladu, *J. Mol. Liq.*, **230**, 344 (2017).
47. R.-r. Shan, L.-g. Yan, K. Yang, S.-j. Yu, Y.-f. Hao, H.-q. Yu and B. Du, *Chem. Eng. J.*, **252**, 38 (2014).
48. A. Khalid, M. Zubair and Ihsanullah, *Arabian J. Sci Eng.*, **43**, 2167 (2018).
49. W. Yao, S. Yu, J. Wang, Y. Zou, S. Lu, Y. Ai, N. S. Alharbi, A. Alsaedi, T. Hayat and X. Wang, *Chem. Eng. J.*, **307**, 476 (2017).
50. J. Wang, D. Kang, X. Yu, M. Ge and Y. Chen, *Chem. Eng. J.*, **264**, 506 (2015).
51. Q. Zhou, F. Chen, W. Wu, R. Bu, W. Li and F. Yang, *Chem. Eng. J.*, **285**, 198 (2016).
52. N. Dizge, C. Aydiner, E. Demirbas, M. Kobya and S. Kara, *J. Hazard. Mater.*, **150**, 737 (2008).
53. Z. Jin, X. Wang, Y. Sun, Y. Ai and X. Wang, *Environ. Sci. Technol.*, **49**, 9168 (2015).
54. W. Xiang, G. Zhang, Y. Zhang, D. Tang and J. Wang, *Chem. Eng. J.*, **250**, 423 (2014).
55. S. L. Wang, R. J. Hseu, R. R. Chang, P. N. Chiang, J. H. Chen and Y. M. Tzou, *Colloids Surf., A: Physicochem. Eng. Aspects*, **277**, 8 (2006).
56. P. Ganesan, R. Kamaraj and S. Vasudevan, *J. Taiwan Inst. Chem. Engineers*, **44**, 808 (2013).
57. S. Samuei, Z. Rezvani and A. R. Amani-Ghadim, *Environ. Prog. Sust. Energy*, **36**, 372 (2017).
58. D. Chen, Y. Li, J. Zhang, W. Li, J. Zhou, L. Shao and G. Qian, *J. Hazard. Mater.*, **243**, 152 (2012).
59. L. Ai, C. Zhang and L. Meng, *J. Chem. Eng. Data*, **56**, 4217 (2011).
60. Q. Hu, Z. Xu, S. Qiao, F. Haghseresht, M. Wilson and G. Q. Lu, *J. Colloid Interface Sci.*, **308**, 191 (2007).

Supporting Information

Graphene/Ternary layered double hydroxide composites: Efficient removal of anionic dye from aqueous phase

Taye Saheed Kazeem*, Mukarram Zubair, Muhammad Daud***, Nuhu Dalhat Mu'azu**, and Mamdouh Ahmed Al-Harthi*,****,†**

*Department of Chemical Engineering, King Fahd University of Petroleum & Minerals, Dhahran 31261, Saudi Arabia
**Department of Environmental Engineering, Imam Abdulrahman Bin Faisal University, Dammam 31982, Saudi Arabia
***Department of Chemical Engineering, University of Engineering and Technology, 25120 Peshawar, Pakistan
****Center of Research Excellence in Nanotechnology, King Fahd University of Petroleum & Minerals, 31261 Dhahran, Saudi Arabia

(*Received 6 November 2018 • accepted 27 April 2019*)

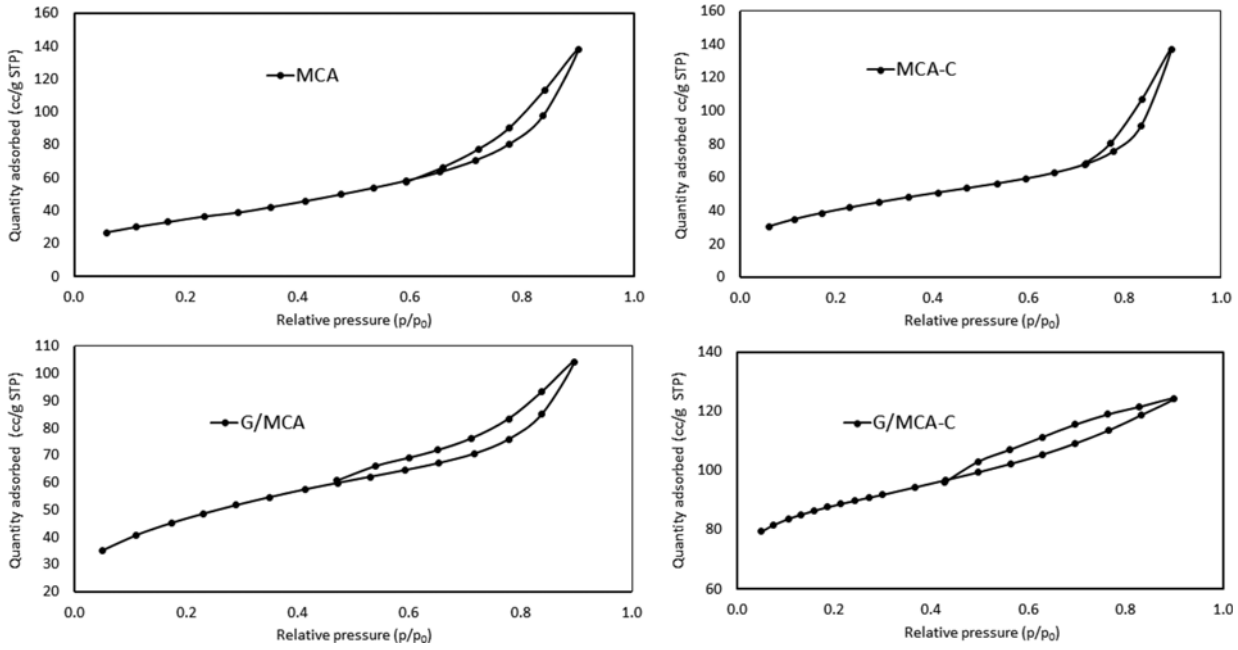

Fig. S1. Isotherm plots of N2 physisorption for MCA, G/MCA, MCA-C, and G/MCA-C.

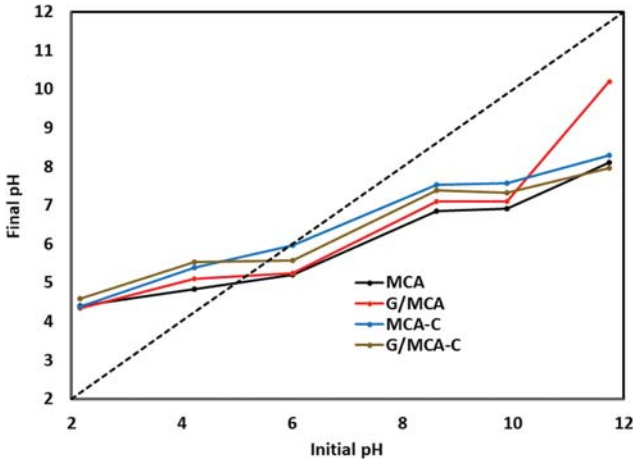

Fig. S2. pH_{PZC} for MCA, G/MCA, MCA-C, and G/MCA.